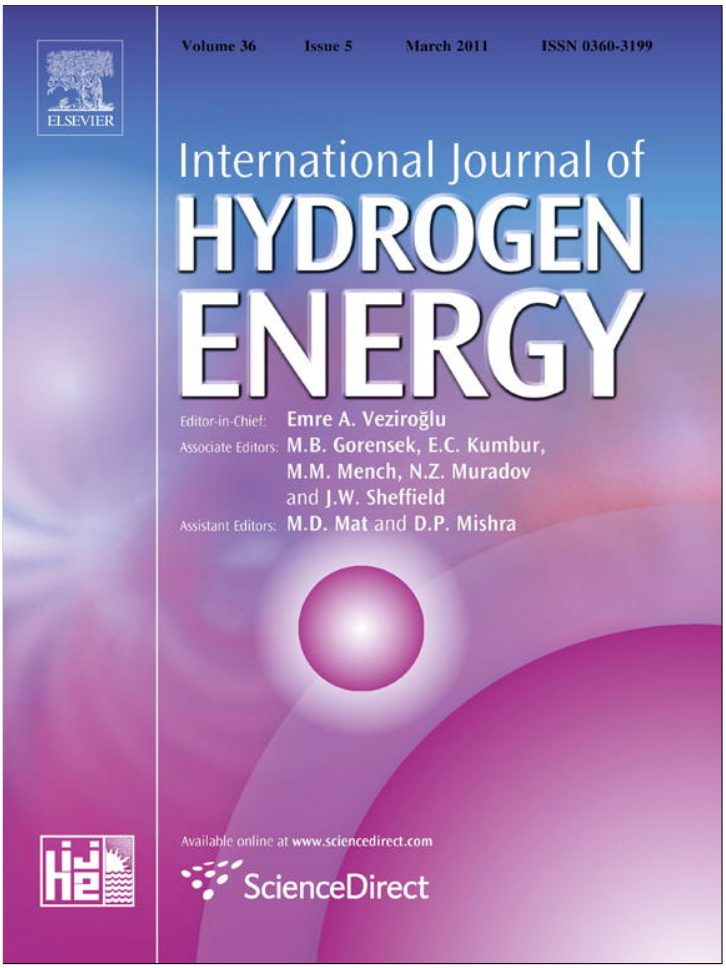

INTERNATIONAL JOURNAL OF HYDROGEN ENERGY 36 (2011) 3313–3321

Available at www.sciencedirect.com

ScienceDirect

journal homepage: www.elsevier.com/locate/he

Nanostructured Pt and Pt–Sn catalysts supported on oxidized carbon nanotubes for ethanol and ethylene glycol electro-oxidation

J.M. Sieben[*,1], *M.M.E. Duarte*[2]

Instituto de Ingeniería Electroquímica y Corrosión (INIEC), Universidad Nacional del Sur. Av. Alem 1253, (B8000CPB) Bahía Blanca, Argentina

ARTICLE INFO

Article history:
Received 5 October 2010
Received in revised form
3 December 2010
Accepted 4 December 2010
Available online 3 January 2011

Keywords:
Pt–Sn alloys
Nanostructured catalysts
Electrodeposition
Ethanol and ethylene glycol electro-oxidation

ABSTRACT

Pt and Pt–Sn catalysts supported on oxidized carbon nanotubes were prepared by multiple potentiostatic pulses and tested for ethanol and ethylene glycol electro-oxidation in sulfuric acid. The composed nanostructured materials were characterized via SEM, TEM, EDX and XRD analysis. Small metal nanoparticles (4–6 nm) forming 3-D nanostructured agglomerates (25–100 nm) distributed over the carbon substrate were formed. XRD results showed that the bimetallic electrocatalysts consisted of a Pt single-phase material, suggesting the formation of solid solutions over the entire composition range. The tin content in the alloys was between 10 and 40 at. %.

Cyclic voltammetry and chronoamperometry measurements at room temperature showed that at potentials below 0.5 V, the bimetallic catalyst with 40 at. % Sn exhibited the highest activity for ethanol and ethylene glycol oxidation, whereas at potentials above 0.5 V, the alloy with 25 at. % Sn displayed better performance. This behavior can be explained by the synergistic effect between the facilitation of alcohol oxidation via oxygen-containing species adsorbed on Sn atoms, the alteration of the electronic structure of Pt atoms that weakens CO and intermediates adsorption, and the adequate Pt ensembles size. Besides, the increment of the lattice parameter and the presence of grain boundaries can enhance the adsorption of the alcohols and favor the splitting of the C–C bond.

1. Introduction

Direct methanol fuel cells (DMFC) are considered to be the most promising energy devices for mobile and stationary applications such as cellular phones, laptop computers and secondary electricity generators [1]. However, methanol presents some safety risks such as high toxicity and inflammability. Besides, methanol crossover through ionomeric membranes cannot be avoided [2,3]. These reasons lead to find some alternative fuel as ethanol (EtOH) or ethylene glycol (EG), which appear to be potentially more attractive due to their non-toxicity, low volatility, high energy density, together with less pronounced crossover due to their larger molecular size [4,5].

Nowadays, the main problem of direct alcohol fuel cells (DAFC) is the deficient activity and selectivity of anode electrocatalysts at temperatures compatible with available membranes. Platinum is the best catalyst for alcohol oxidation, but its surface is rapidly poisoned by strongly irreversibly

* *Corresponding author*. Tel./fax: +54 291 4595182.
E-mail address: jmsieben@uns.edu.ar (J.M. Sieben).
[1] Member of CONICET – Argentina.
[2] Member of CIC – Argentina.

0360-3199/$ – see front matter
doi:10.1016/j.ijhydene.2010.12.020

adsorbed CO-like intermediates coming from the dissociative adsorption of alcohols. Besides, the splitting of the C–C bond is the main obstacle in ethanol and ethylene glycol electro-oxidation. Efforts to diminish these problems have been concentrated on the addition of more oxophilic co-catalysts, forming bi- and tri-metallic alloys of Pt with elements as Ru, Sn, Mo, W, Ni, Os, Pd, Co, Au and Rh [6–15]. Additionally, because alcohol oxidation reactions are known to be structure sensitive, it is important to consider the dispersion, particle size and morphology, and degree of alloying of Pt-based catalyst at nanoscale level [16,17].

The manufacture of Pt-based nanostructured bi- or tri-metallic catalysts by electrochemical techniques presents several advantages, since it is a simple operation, of low cost, that permits obtaining deposits of high purity and uniform deposition. Besides, the catalyst structure, dispersion and particle size can be controlled in some extent by the selection of current density or overpotential, which determine the number and size of the nanoparticles [18–22]. In this method, the metal particles can be deposited selectively at desired locations in the electrode, since the technique requires both ionic and electronic access. On the other hand, it does not require heat treatments (oxidative and/or reducing), as most chemical methods, in order for example to clean the catalytic particles from surfactant contamination.

Bimetallic Pt–Sn carbon supported systems are known to exhibit high catalytic activity for ethanol oxidation in acid media. The presence of Sn alters the electronic structure of Pt, weakening CO adsorption on the Pt surface, thus reducing catalyst poisoning [5,23,24]. Besides, $Sn(OH)_2$ or $Sn(OH)_4$ provides OH_{ads} species by dissociating water at a lower potential that on Pt, and these OH_{ads} species are helpful for the subsequent oxidation of adsorbed intermediates (bifunctional mechanism [25]) to acetaldehyde, acetic acid, and CO_2 [6,26–28].

At the present time, it is well known that the preparation procedure affects the characteristics of the deposits (particle dispersion, composition, etc.). However the optimum Sn content is not well determined and depends on temperature, potential range and type of catalyst. Lamy et al. [27] and Lycke et al. [29] found that the optimum tin content in Pt–Sn/C catalysts was in the range of 10–20 at. % Sn for ethanol oxidation at room temperature, while Spinace et al. [9] and Xin et al. [30] observed better activities for catalysts with 50 and 33–50 at. % Sn respectively, indicating a strong dependence on its preparation procedure. On the other hand, Zhou et al. [11] and Tsiakaras [10] reported that a Pt–Sn alloy containing 33 at. % Sn is most suitable for ethanol oxidation between 60 °C and 90 °C.

In the present work, the role of the structural features of Pt–Sn electrodeposited catalysts in the electro-oxidation of ethanol and ethylene glycol was analyzed. Pt and Pt–Sn nanostructured materials of different compositions were prepared by multiple cycles of potentiostatic pulses onto oxidized multi-walled carbon nanotubes (O-MWCNTs). Physical property characterizations were carried out to investigate the microstructure, dispersion and degree of alloying of Sn in the bimetallic catalysts. In addition, the electrochemical activity of the catalysts for ethanol and ethylene glycol electro-oxidation was evaluated by cyclic voltammetry and chronoamperometry.

2. Experimental

Glassy carbon (GC) discs of 0.07 cm^2 exposed geometric area were coated by a layer of oxidized multi-walled carbon nanotubes (O-MWCNTs) using electrophoretic deposition (EPD). The nanotubes were oxidized in 40 ml of a 3:1 mixture of concentrated H_2SO_4/HNO_3, refluxing at about 120 °C for 45 min. Afterward they were washed with bidistilled water until a neutral pH was reached, and sonicated for 60 min to obtain a well dispersed suspension of 3.3 mg ml^{-1}. Under these conditions defective sites in the MWCNTs are functionalized, resulting in the formation of fragmented MWCNTs decorated with carboxylic acid and other oxygen-containing groups on their surface. These acidic groups electrostatically stabilize the CNTs in water by developing a negative surface charge [31]. The EPD deposition was carried out in a cell with two parallel electrodes separated 1 cm, applying a constant DC potential (10 V) for 5 min using a stabilized power supply (Oltronix C40-08D). Then, the electrodes were left to dry for a day previously to metal electrodeposition.

Conventional three-compartment glass cells were used to run the electrochemical experiments at room temperature with a PAR 273 potentiostat/galvanostat. The counter-electrode was a platinum foil, and a saturated calomel electrode (SCE) served as reference. All potentials mentioned in this work are referred to this electrode. An inert nitrogen atmosphere was maintained over the electrolyte. Electrochemical techniques such as cyclic voltammetry and chronoamperometry were used to characterize the catalysts and to study the ethanol and ethylene glycol electro-oxidation.

The catalysts were synthesized by electrodeposition at 25 °C using freshly prepared diluted solutions of 2 mM H_2PtCl_6 + X mM $SnCl_2$ (X = 0, 2, 4 and 6) in 0.5 M H_2SO_4. The electrodeposition was carried out using multiple successive potentiostatic pulses ($E_{cathodic}$ = −0.5 V $t_{cathodic}$ = 5 s, E_{anodic} = 0.5 V t_{anodic} = 5 s), applying 15 consecutive cycles. After deposition, the electrodes were thoroughly rinsed with bidistilled water and tested in sulfuric acid solution using cyclic voltammetry (sweep rate 50 mV s^{-1}).

The active surface area of the electrocatalysts was determined by copper underpotential deposition (Cu-UPD). Experimental details have been described in a previous paper [32].

The electrode activity for ethanol and ethylene glycol electro-oxidation was measured in 1 M EtOH or EG + 0.5 M H_2SO_4 solution by applying a potential sweep at a scan rate of 50 mV s^{-1}. Chronoamperometry curves were obtained applying potentials pulses for 15 min from an initial potential of 0 V. Current densities for ethanol and ethylene glycol oxidation were normalized per milligram of Pt.

The morphology of the catalyst surface and the particle size were analyzed using SEM (EVO 40 LEO) and TEM (JEOL, 100CX II) microscopies. The structure of the electrodes was characterized by X-ray diffraction (XRD) using a Rigaku D_{max} III C diffractometer with monochromated CuKα radiation source operated at 40 keV at a scan rate of 0.05°s^{-1}. Bulk composition analysis was performed by an energy dispersive spectroscopy (EDX) probe attached to a SEM microscope (JEOL 100).

The amount of Pt deposited on the substrate was estimated using ICP-AES (Shimadzu 1000 model III). The samples were

prepared by digesting the electrodes in boiling aqua regia and then removing excess acid.

3. Results and discussion

3.1. Characterization of supported Pt–Sn catalysts

Fig. 1 shows the cyclic voltammetry curves for the different catalysts/O-MWCNTs in absence of alcohol. The voltammograms corresponding to Pt–Sn catalysts did not display a well-defined hydrogen adsorption/desorption zone, conversely to the case of Pt, and the current densities in the double layer region were larger than those on pure platinum. This behavior is characteristic of bimetallic catalysts containing oxophilic transition metals as Sn, Ru, Os and Mo [7,8]. The increase of the tin content in the bimetallic Pt–Sn catalysts leaded to an important increase in the double layer charge, along with the appearance of a cathodic peak at about 0.25 V that augments with increasing Sn content, which could be related to tin oxide and hydroxy species formation [9].

Fig. 2(a) shows the EDX spectra of a Pt–Sn catalyst prepared by multiple potentiostatic pulses in a solution containing 2 mM H_2PtCl_6 and 6 mM $SnCl_2$. Bulk Sn contents of 10, 25 and 40 at. % were measured by EDX for the bimetallic catalysts prepared from platinum–tin solutions of mol ratio 1:1 (PS1), 1:2 (PS2) and 1:3 (PS3), respectively.

XRD diffraction patterns of Pt and Pt–Sn catalysts are shown in Fig. 2(b). The characteristics extracted from the diffractograms are summarized in Table 1. The small intensity peak observed in the diffraction patterns at $2\theta \approx 42^\circ$ can be assigned to plane of graphite (100). All catalysts presented the typical features of the Pt face centered cubic (fcc) phase. The three reflections peaks at about 40, 46 and 68° of 2θ values, which are associated with the Pt (111), (200) and (220) planes respectively, indicated that the bimetallic catalysts have single-phase arrangement. Particularly, the Pt (111) peak, the highest intensity peak for all catalysts, appeared at 2θ values varying between 38.5° and 39.9°, which corresponded to d spacing in the range of 2.338–2.264 Å. Compared with the reflections of Pt/O-MWCNTs catalyst (P), the diffraction peaks for the bimetallic Pt–Sn catalysts were slightly shifted to lower 2θ values. The slight shift of the diffraction peaks revealed the formation of a solid solution involving the incorporation of Sn atoms into the fcc lattice of Pt. Besides, the diffraction peaks at 33.9, 51.8 and 65° indicative of the presence of SnO_2 phase were not observed, but their presence cannot be discarded because they may be present in very small amount or even in amorphous form. Furthermore, the ratio between (111) and (220) areas does not change appreciably in these samples indicating the absence of any preferential orientation.

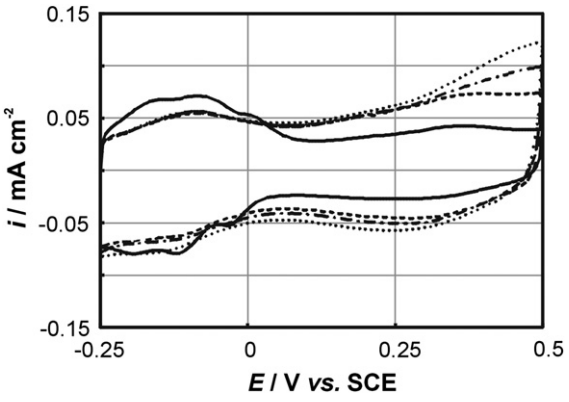

Fig. 1 – Cyclic voltammograms for Pt/O-MWCNTs and Pt–Sn/O-MWCNT in 0.5 M H_2SO_4 at room temperature. Pt (—), and Pt–Sn mol ratio 1:1 (– •), 1:2 (–••), 1:3 (····). Sweep rate 50 mV s^{-1}.

The fitting of the XRD raw data for these supported catalysts only required the Pt fcc phase, that is, the addition of a Sn phase was not needed, thus being consistent with the view that Sn is totally dissolved in the Pt fcc lattice. The peak profiles in XRD patterns of the catalysts were fitted with the pseudo-Voigt function, using non-linear least-squares refinement procedures based on a finite difference Marquardt algorithm. Using the peak (111) of the fcc structure, which is not influenced by the broad peak of the carbon support located at $2\theta \approx 26^\circ$ (not shown), the lattice parameters were estimated using Bragg's law and the particle sizes estimated using Scherrer's equation.

The lattice parameter of Pt/O-MWCNTs was slightly lower than that of pure Pt (3.923). This could either be due to the small size of the particles [33], or to Pt-support interactions [34], being the latter reason most suitable for this case. The lattice parameters of Pt–Sn bimetallic catalysts were different from each other, increasing with the Sn content as shown in Table 1. The addition of Sn, which has a larger atomic radius than Pt (1.61 Å against 1.39 Å), induces the stretching of the Pt fcc lattice. In fact, the increase in lattice parameter of the alloy catalysts reflects the progressive increase in the incorporation of Sn into the alloyed state. From the values of the lattice parameter, the atomic fraction of Sn in the Pt–Sn alloy can be assessed, assuming that the Pt–Sn lattice parameter of the supported bimetallic alloy follows the Vegard's law [35]:

$$X_{Sn} = \frac{a_{Pt-Sn} - a_{Pt}}{0.352} \quad (1)$$

where, a_{Pt} is the lattice parameter of Pt, a_{Pt-Sn} is the lattice parameter of Pt–Sn alloys and X_{Sn} is the atomic fraction of Sn. In accordance with the Vegard's law, the nominal Sn contents in the Pt–Sn/O-MWCNTs catalysts estimated from XRD patterns agree with those measured from EDX analysis.

Additionally Debye–Scherrer's equation (Eq. (2)) was used to estimate the average Pt–Sn crystallite size from the most distinct peak, Pt (111) centered at 2θ values between 38.5° and 39.9° (Fig. 2(c)):

$$d_C = \frac{0.9\lambda_{K\alpha 1}}{B_{(2\theta)}\cos\theta_B} \quad (2)$$

where, $\lambda_K\alpha_1$ is the wavelength of X-ray, θ_B is the angle of (111) peak, and $B_{(2\theta)}$ is the full width at half-maximum (FWHM) of the peak broadening in radians and the value 0.94 comes from considering spherical crystallite geometry (cubo-octahedral shape). The size of the crystallites d_c (nm) (more properly, the coherence length of crystalline domains) measured from diffractograms are listed in Table 1. The average size of the

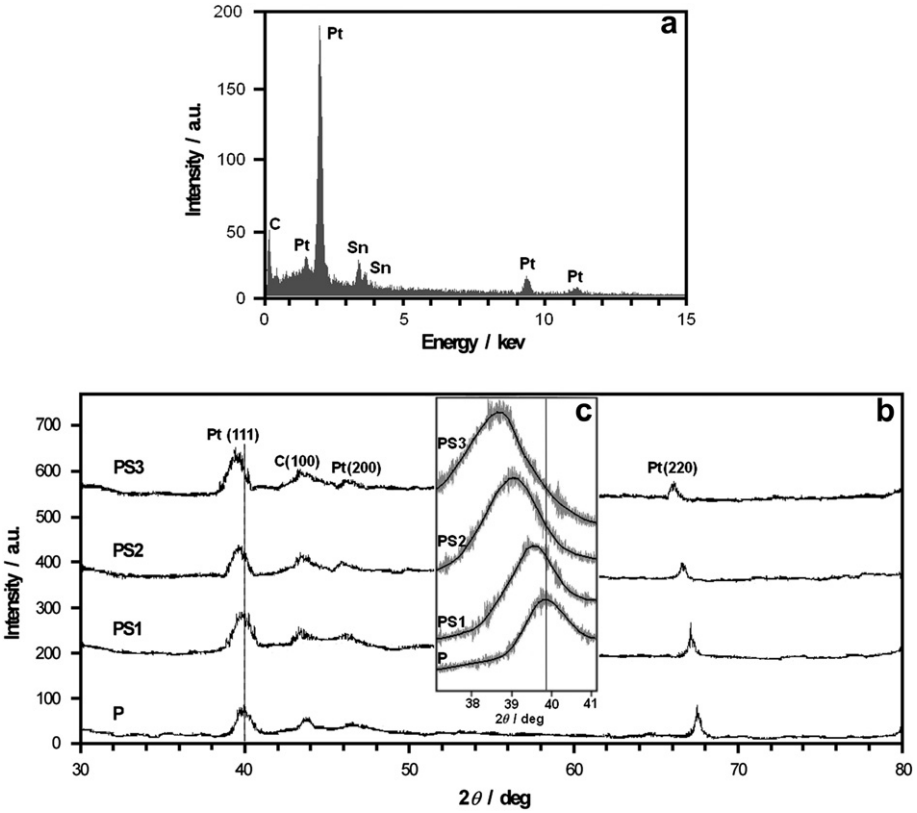

Fig. 2 – (a) EDX spectra for the bimetallic Pt–Sn catalyst with 40 at. % Sn supported on O-MWCNTs. (b) XRD patterns of Pt/O-MWCNTs and Pt–Sn/O-MWCNTs electrocatalysts. The inset (c) shows the fine scanning about the (111) reflection plane of the Pt and Pt–Sn clusters: raw data (▬) and deconvoluted profiles (▬).

crystallites was found to be between 2 and 3.5 nm, in accordance with the sizes obtained by Gupta et al. [36] with electrodes prepared by galvanostatic electrodeposition. These results imply that the electrodeposition method was able to produce small crystallites, even at relatively large amounts of electrodeposited Pt and Pt–Sn. In addition, XRD results indicate that the catalyst crystallite size slightly increases as the Sn content augments.

A SEM micrograph of the EPD deposited multi-walled carbon nanotubes is shown in Fig. 3(a), while Fig. 3(b) shows the TEM image of the catalyst PS3 (40 at. % Sn). At first inspection, the electrochemical pulsed technique here used generated rough 3-D semispherical agglomerates with sizes in the range of 50–100 nm, although agglomerates with smaller sizes (between 10 and 25 nm) were also observed. These agglomerates seemed to be formed by irregular nanoparticles with diameters between 4 and 5 nm (slightly larger than those estimated from XRD analysis). Hence, the aggregates may rather be visualized as disordered nanoclusters of catalyst particles than as large particles with a rough surface. Besides, some extent of dendritic growth was observed on the bigger 3-D aggregates. This behavior can be explained considering that electrodeposition of platinum occurs through 3-D nucleation and growth mechanisms [37,38], where primary nucleation on

Table 1 – Parameters of Pt and Pt–Sn catalysts supported on O-MWCNTs.

Electrode	X_{Sn} (EDX)	[a] a_{fcc}/Å	[b] X_{Sn} (XRD)	[c] d_c/nm	[d] w_{Pt}/mg cm^{-2}	[d] w_{Sn}/mg cm^{-2}	[e] S_w/m^b g^{-1}	$S_{w,cal}$/m^b g^{-1}	ε
P	–	3.9206	–	2.3	0.113	–	47.1	121.6	0.61
PS1	0.10	3.9452	0.07	2.6	0.101	0.006	47.6	112.8	0.58
PS2	0.25	3.9980	0.22	3.2	0.096	0.017	43.3	102.2	0.58
PS3	0.40	4.0508	0.37	3.5	0.090	0.024	45.7	105.7	0.57

a ± 0.0004 Å.
b Estimated from lattice parameter using the Vegard's law (Eq. (1)).
c Determined from Debye–Scherrer equation (Eq. (2)).
d Determined from ICP-AES measurements and expressed per unit of GC geometric area.
e Specific surface area.

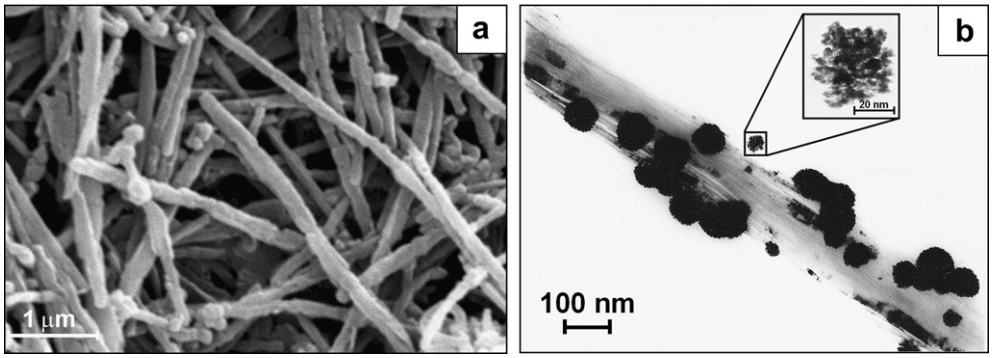

Fig. 3 – SEM image of the oxidized multi-walled carbon nanotubes (O-MWCNTs) deposited by EDP on glassy carbon (GC) (a), and TEM image of the alloy PS3 on O-MWCNTs (b). The inset shows a magnified image of a representative nanoparticle.

carbon is followed by secondary nucleation on the preformed nuclei [39], leading to highly defective nanograined Pt structures [40,41]. On the other hand, the appearance of sharp needles could be due to a faster diffusion rate of the metal ions at the tips of the nano-sized particles under mass-transfer or mixed control conditions [42]. Moreover, Gloaguen et al. [37] and Zoval et al. [38] observed that Pt electrodeposition on a smooth HOPG surface takes place via formation of particles 10–20 nm in diameter followed by lateral sticking through surface diffusion, which results in the formation of agglomerates.

Similar deposit structure, particle size (more properly agglomerate size) and morphology were observed with the other catalysts (not shown). So, particle size effect can be excluded from influential parameters for the electrocatalytic activity over the O-MWCNTs supported Pt–Sn materials.

The specific surface area values of the catalysts are reported in Table 1. It can be seen that S_w is slightly affected by the presence of Sn in the supported bimetallic catalyst.

$$S_w = \frac{S}{w} \tag{3}$$

where, S (m^2) is the active surface area determined from Cu-UPD measurements, and w (g) is the catalyst mass estimated from ICP-AES analysis.

Alternatively, the specific surface area of the metal ($S_{w,cal}$) in the absence of any screening or coalescence of crystals, i.e. assuming homogeneously distributed and spherical or cubic particles, can be calculated from the mean crystallite size determined by XRD [40,43]:

$$S_{w,\,cal} = \frac{6 \times 10^4}{\rho\, d_C} \tag{4}$$

The catalyst density ρ can be assessed using the lattice parameter as follows:

$$\rho = \frac{\text{Unit cell weight}}{\text{Unit cell volume}} = 4 \times 10^{24}\left[\frac{X_{Pt}M_{Pt} + X_{Sn}M_{Sn}}{a_{fcc}^3 N_A}\right] \tag{5}$$

where, ρ (g cm^{-3}) is the density of Pt–Sn alloy, X_{Pt} and X_{Sn} are the atomic fractions of Pt and Sn, M_{Pt} and M_{Sn} are the molecular weights (g mol^{-1}), a_{fcc} (Å) is the lattice parameter and N_A is the Avogadro number. It should be noted from the specific surface area calculated from XRD considerably exceeds the value obtained from Cu stripping and ICP analysis. This behavior can be explained by particle agglomeration at the experimental conditions used to prepare the catalysts. The degree of particle coalescence ξ [40] can be estimated from Eq. (6):

$$\xi = 1 - \frac{S_w}{S_{w,\,calc}} \tag{6}$$

The calculation gives ξ values ca. 0.6, indicating high degree of particle agglomeration. Therefore, part of the nano-sized particle surface will be scarcely accessible to the solution, explaining the low value of specific surface area determined by Cu stripping and ICP-AES measurements. Notwithstanding, ξ can also be used as an indirect measure of the concentration of the grain boundaries regions. So, high density of grain boundaries should be expected for these electrocatalysts, since electrodeposition leads to the formation of defective multilayered structures. In this way, these nanostructured catalysts could be outlined as nano-sized metal grains interconnected via grain boundaries, resulting in the formation of multi-grained structures. According to the recent molecular-dynamics simulations of the structure and deformation behavior of nano-crystalline materials performed by Wolf et al. [44], nanostructured materials may be represented as consisting of highly ordered crystalline domains surrounded by disordered region of about 0.5 nm wide. These discontinuities in the crystal planes may act similarly to low coordinated sites (steps and kinks) on single crystalline and other extended surfaces, which exhibit very high catalytic activity for methanol oxidation [40,41]. Metal atoms in close proximity to the grain boundaries usually have decreased number of neighbors in the first coordination shell, and thus, are expected to bind adsorbates and catalyze bond-breaking reactions.

3.2. *Ethanol and ethylene glycol oxidation on Pt and Pt–Sn/O-MWCNTs*

Fig. 4 shows the cyclic voltammetry curves recorded for ethanol (a) and ethylene glycol (b) at the nanostructured electrodes at room temperature. The oxidation ethanol began above 0 V for the bimetallic catalysts with high Sn content (PS2 and PS3), while the onset potential was shifted toward higher potentials for the catalysts PS1 (~0.1 V) and P (~0.2 V). The

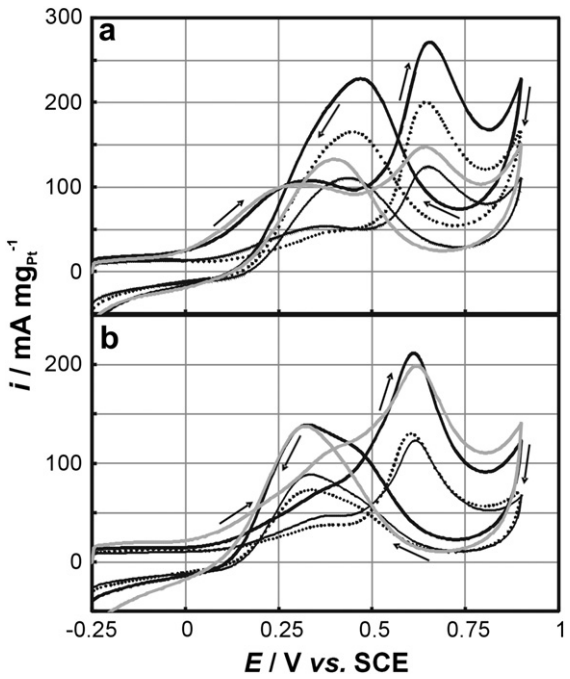

Fig. 4 – Cyclic voltammograms (tenth cycle) for the different electrodes in 1 M CH_3CH_2OH/0.5 M H_2SO_4 (a), and 1 M $OHCH_2CH_2OH$/0.5 M H_2SO_4 (b) at room temperature. Electrode: P (♦♦♦♦♦), PS1 (▬▬), PS2 (▬▬) and PS3 (▬▬). The sweep rate was 50 mV s^{-1} and the arrows indicate the scan direction.

displacement in the beginning of the alcohols electro-oxidation can be associated with the formation of OH_{ads} species on Sn atoms originating in the water dissociation that occurs at more negative potentials that on Pt atoms, through the so called bifunctional mechanism [25].

On the other hand, the onset of EG oxidation for all the catalysts was shifted about 0.1 V to more positive potential values than those observed for EtOH oxidation. Furthermore, it could be seen that the catalytic activities (current densities) for EtOH oxidation were slightly greater than that observed for EG oxidation. This behavior may be related to the difference in their adsorption behavior on the catalyst surfaces at the potential region between 0 and 0.25 V [45].

In addition, two oxidation peaks during the forward scan and one oxidation peak during the backward scan could be observed for both EtOH and EG oxidation in all the electrodes. After passing the second peak in the forward scan the current decays continuously, and then starts to increase again at potentials higher than 0.8 V due to the formation of incomplete oxidation products, e.g. formation of acetaldehyde and acetic acid for ethanol oxidation [46]. Additionally, the backward peak for EG oxidation was accompanied by a wide shoulder. The identity of the products associated with the peaks observed in the voltammograms are still today under discussion. Friedrich et al. [47] by using differential electrochemical mass spectroscopy (DEMS) and cyclic voltammetry concluded that the first peak for ethanol oxidation on Pt–Ru catalysts corresponds mainly to the formation of CO_2, whereas the second peak corresponds mainly to the formation of CH_3CHO. Moreover, the presence of adsorbed CO and CH_3COOH as a stable product were reported by several groups by means of infra-red spectroscopy (FTIR) [27,48], DEMS [49,50] and ion or liquid chromatography [51,52]. On the other hand, Wang et al. [53] using DEMS disclosed that EtOH oxidation on Pt/C, Pt–Ru/C and Pt–Sn/C catalysts leads to the formation of CO_2 (first peak), and mainly to the formation CH_3CHO and CH_3COOH (second peak). Besides, Wang et al. [54] also studied EG electro-oxidation on a Pt/C catalyst. They concluded that EG oxidation at low potentials (first peak zone) leads to the formation of C2 by-products (predominantly glycolic and oxalic acids) and EG dissociation to CO_{ads}, while the oxidation at high potentials (second zone) leads to the formation of CO_2. In addition, glycolaldehyde as well as glyoxylic acid and glyoxal were identified by using FTIR and ion chromatography [55,56]. Moreover, the reverse anodic peak observed in the electro-oxidation of both alcohols can be attributed to the oxidative removal of incompletely oxidized carbonaceous species formed in the forward scan.

The ratio of the coulombic charges associated with the anodic peaks in the forward and in the reverse scans can be used as a qualitative measure of the fraction of the catalyst surface that is free from the accumulation of ethanolic and glycolic residues. From Table 2 it can be seen that Q_f/Q_b becomes greater when the Sn content increases in the alloy, indicating a better tolerance to poisoning.

Below 0.5 V the bimetallic catalysts PS2 and PS3 exhibit the maximum activities for EtOH and EG oxidation, being the performance of PS3 similar and slightly greater than that of PS2 for EtOH and EG oxidation, respectively (PS3 ≥ PS2 > PS1 > P). At potentials above 0.55 V PS2 prevails as the best catalyst for the electro-oxidation of both alcohols, reaching the highest forward peak current density. Moreover, the catalyst PS3 maintains the second greater current density for EG oxidation (PS2 > PS3 > P > PS1), but it is surpassed by catalyst P at potentials higher than 0.55 V for ethanol electro-oxidation (PS2 > P > PS3 >PS1).

As was mentioned previously, the behavior of the catalysts in the first peak zone (<0.50 V) can be related to the facilitation of alcohol oxidation via oxygen-containing species (OH_{ads}) adsorbed on Sn atoms. Additionally, the modification of the electronic structure of Pt atoms, caused by charge transfer from the less electronegative Sn to the more electronegative Pt in the solid solution, can reduce CO and intermediates adsorption on the platinum surface, limiting catalyst poisoning [20]. Besides, the increment of the lattice parameter [11,57] and the presence of high density of grain boundaries

Table 2 – Ratio of the coulombic charges associated with the anodic peaks in the forward scan (Q_f) and in the reverse scan (Q_b) from voltammetric data for EtOH and EG electro-oxidation.

Electrode	EtOH	EG
	Q_f/Q_b	Q_f/Q_b
P	0.56	0.78
PS1	0.51	0.76
PS2	0.78	0.82
PS3	0.93	0.99

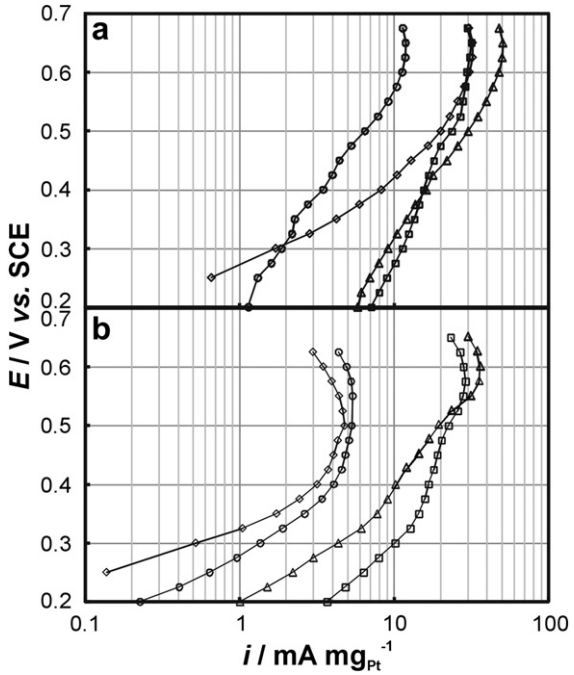

Fig. 5 – Tafel plot at 25 °C for the different electrodes in 1 M CH_3CH_2OH/0.5 M H_2SO_4 (a), and 1 M $OHCH_2CH_2OH$/0.5 M H_2SO_4 (b). Electrodes: P (-◇-), PS1 (-○-), PS2 (-△-) and PS3 (-□-). Data taken from chronoamperometry experiments at various potentials after 15 min.

[40,41] can enhance the adsorption of the alcohols and can favor the splitting of the C–C bond, improving EtOH and EG utilization and consequently the performance of PS2 and PS3, since C–C and C–O cleavage are known to be sensitive to specific geometric arrangements of the surface metal atoms, affecting parameters as bond length and angles [58]. Conversely, at low tin content there will be not enough Sn sites to modify the electronic and geometric structure of Pt and to supply the OH_{ads} species.

On the other hand, the behavior of the catalysts for potentials greater than 0.5 V (second peak zone) can be rationalized considering the existence of a compromise between the available Pt sites for producing the dissociative adsorption of the alcohols and the C–C bond-breaking reaction along with the amount of OH_{ads} species on Sn atoms capable of promoting the complete oxidation of the carbonaceous residues. Additionally, at potentials greater than 0.55 V the OH_{ads} groups can be also formed on atoms of Pt, improving the ability of P catalyst to oxidize CO_{ads} intermediary at room temperature. So, the low catalytic activity of PS3 compared to P catalyst for ethanol oxidation can be due to the reduction of available Pt sites by Sn species and the lack of the required Pt ensembles size to accommodate the resulting carbonaceous fragments, i.e. an adequate geometric distribution of neighboring Pt sites on the catalyst surface [53].

Similar Sn requirement is observed for EtOH and EG oxidation within the potential range of technical interest (<0.55 V 40 at. %Sn), but some differences were observed in the second peak zone as was commented previously. It is interesting to note that EG appear to need different Pt sites arrangement, than in the case of EtOH oxidation, to hold the alcohol fragments on the catalyst surface. In other words, larger Pt ensembles may be required to oxidize ethanol compared to ethylene glycol reaction. This interpretation can be inferred from voltammetric experiments, where PS3 exhibited greater and similar current densities that on PS2 catalyst at potentials below and above 0.55 V, respectively. Whereas the catalyst with 40 at. % Sn exhibited similar and lower current densities than those for the catalyst with 25 at % Sn at potentials beneath and over 0.55 V, respectively. An alternative explanation to such comportment can be also proposed, since a different OH_{ads} requirement to fully oxidize both alcohols may be involved during the electro-oxidation process. However, more experiments should be required to confirm such remark. So, this issue along with the kinetic evaluation of both processes will be the object of a further work.

The comparative catalytic activity of the electrodes was determined from polarization curves and the corresponding Tafel plots (Fig. 5). Chronoamperometry tests were carried out at room temperature in a range of potentials between 0.2 and 0.65 V, and each measurement was extended over 15 min to attain quasi-steady state conditions. The Tafel plots largely reproduce the catalytic performance observed in the voltammetric curves, but with lower current densities due to the partial blocking of the active sites by accumulation of poisoning species over the entire potential range.

4. Conclusions

In this work well-alloyed Pt–Sn carbon supported catalysts synthesized by pulse electrodeposition over oxidized carbon nanotubes were evaluated as materials for ethanol and ethylene glycol electro-oxidation. The optimum Pt:Sn composition for ethanol and ethylene glycol oxidation within the potential range of practical interest was 3:2 (40 at. % Sn), while at higher potentials was 4:1 (25 at. % Sn). This behavior can be explained considering the synergistic effect between the facilitation of alcohol oxidation via oxygen-containing species adsorbed on Sn atoms, the alteration of the electronic structure of Pt atoms that weakens CO and intermediates adsorption, and the adequate Pt ensembles size. Moreover, the increment of the lattice parameter and the presence of grain boundaries can enhance the adsorption of the alcohols and favor the splitting of the C–C bond.

The electrochemical preparation technique described above leaded to electrodes with good catalytic activities for both ethanol and ethylene glycol electro-oxidation in the potential range useful for practical applications.

Acknowledgements

This work was supported by ANPCYT grant No 10-11133, UNS grant 24/M097 and CIC. J.M.S. is grateful to Graciela Mas for her assistance in the XRD measurements.

REFERENCES

[1] Iwasita T. In: Vielstich W, et al., editors. Handbook of fuel cells Fundamentals, Technology and applications, Vol. 2. New York: John Wiley & Sons; 2003.

[2] Wei ZD, Chan SH. Electrochemical deposition of PtRu on an uncatalyzed carbon electrode for methanol electrooxidation. J Electroanal Chem 2004;569:23–33.

[3] Song JM, Miyatake K, Uchida H, Watanabe M. Investigation of direct methanol fuel cell performance of sulfonated polyimide membrane. Electrochim Acta 2006;51:4497–504.

[4] An L, Zhao TS, Shen SY, Wu QX, Chen R. Performance of a direct ethylene glycol fuel cell with an anion-exchange membrane. Int J Hydrogen Energy 2010;35:4329–35.

[5] Rousseau S, Coutanceau C, Lamy C, Léger J- M. Direct ethanol fuel cell (DEFC): electrical performances and reaction products distribution under operating conditions with different platinum-based anodes. J Power Sourc 2006;158:18–24.

[6] Anderson AB, Seong S, Grantscharova E. Molecular orbital investigation of water reactions with tin hydroxide complexes in association with platinum electrodes. J Phys Chem 1996;100:17535–8.

[7] Antolini E, Colmati F, González ER. Effect of Ru addition on the structural characteristics and the electrochemical activity for ethanol oxidation of carbon supported Pt–Sn alloy catalysts. Electrochem Commun 2007;9:398–404.

[8] Barroso de Oliveira M, Profeti LPR, Olivi P. Electrooxidation of methanol on PtM_yO_x (M = Sn, Mo, Os or W) electrodes. Electrochem Commun 2005;7:703–9.

[9] Spinace EV, Linardi M, Oliveira Neto A. Co-catalytic effect of nickel in the electro-oxidation of ethanol on binary Pt-Sn electrocatalysts. Electrochem Commun 2005;7:365–9.

[10] Tsiakaras PE. PtM/C (M = Sn, Ru, Pd, W) based anode direct ethanol-PEMFCs: structural characteristics and cell performance. J Power Sourc 2007;171:107–12.

[11] Zhou W, Zhou Z, Song S, Li W, Sun G, Tsiakaras P, et al. Pt based anode catalysts for direct ethanol fuel cells. Appl Catal B 2003;46:273–85.

[12] Kadirgan F, Kannan AM, Atilan T, Beyhan S, Ozenler SS, Suzer S, et al. Carbon supported nano-sized Pt-Pd and Pt-Co electrocatalysts for proton exchange membrane fuel cells. Int J Hydrogen Energy 2009;34:9450–60.

[13] Lopes T, Antolini E, Gonzalez ER. Carbon supported Pt-Pd alloy as an ethanol tolerant oxygen reduction electrocatalyst for direct ethanol fuel cells. Int J Hydrogen Energy 2008;33: 5563–70.

[14] Zhu H, Liu Y, Shen L, Wei Y, Guo Z, Wang H, et al. Microwave heated polyol synthesis of carbon supported PtAuSn/C nanoparticles for ethanol electrooxidation. Int J Hydrogen Energy 2010;35:3125–8.

[15] Shen SY, Zhao TS, Xu JB. Carbon supported PtRh catalysts for ethanol oxidation in alkaline direct ethanol fuel cell. Int J Hydrogen Energy 2010;35:12911–7.

[16] Hoster HE, Iwasita T, Baumgrtner E, Vielstich W. Pt-Ru model catalysts for anodic methanol oxidation: influence of structure and composition on the reactivity. Phys Chem Chem Phys 2001;3:337–46.

[17] Hoster HE, Bergbreiter A, Erne PM, Hager T, Rauscher H, Behm RJ. Pt_xRu_{1-x}/Ru(0001) surface alloys-formation and atom distribution. Phys Chem Chem Phys 2008;10:3812–23.

[18] Löffler MS, Natter H, Hempelmann R, Wippermann K. Preparation and characterisation of Pt-Ru model electrodes for the direct methanol fuel cell. Electrochim Acta 2003;48:3047–51.

[19] Lima A, Coutanceau C, Léger J-M, Lamy C. Investigation of ternary catalysts for methanol electrooxidation. J Appl Electrochem 2001;31:379–86.

[20] Rao CRK, Trivedi DC. Chemical and electrochemical depositions of platinum group metals and their applications. Coord Chem Rev 2005;249:613–31.

[21] Duarte MME, Pilla AS, Sieben JM, Mayer CE. Platinum particles electrodeposition on carbon substrates. Electrochem Commun 2006;8:159–64.

[22] García MF, Sieben JM, Duarte MME, Mayer CE. Methanol/air fuel cells: catalytic aspects and experimental diagnostics. Int J Hydrogen Energy 2008;33:3517–21.

[23] Alcalá R, Shabaker JW, Huber GW, Sanchez-Castillo MA, Dumesic JA. Experimental and Dft studies of the conversion of ethanol and acetic acid on PtSn-based catalysts. J Phys Chem B 2005;109:2074–85.

[24] Colmati F, Antolini E, Gonzalez ER. Ethanol oxidation on carbon supported pt-sn electrocatalysts prepared by reduction with formic acid. J Electrochem Soc 2007;154: B39–47.

[25] Watanabe W, Motoo S. Electrocatalysis by ad-atoms: part II. Enhancement of the oxidation of methanol on platinum by ruthenium ad-atoms. J Electroanal Chem 1975;60:267–73.

[26] Vigier F, Coutanceau C, Hahn F, Belgsir EM, Lamy C. On the mechanism of ethanol electro-oxidation on Pt and PtSn catalysts: electrochemical and in situ IR reflectance spectroscopy studies. J Electroanal Chem 2004;563:81–9.

[27] Song SQ, Zhou WJ, Zhou ZH, Jiang LH, Sun GQ, Xin Q, et al. Direct ethanol PEM fuel cells: the case of platinum based anodes. Int J Hydrogen Energy 2005;30:995–1001.

[28] Chu YH, Shul YG. Combinatorial investigation of Pt-Ru-Sn alloys as an anode electrocatalysts for direct alcohol fuel cells. Int J Hydrogen Energy 2010;35:11261–70.

[29] Lycke DR, Gyenge EL. Electrochemically assisted organosol method for Pt-Sn nanoparticle synthesis and in situ deposition on graphite felt support: extended reaction zone anodes for direct ethanol fuel cells. Electrochim Acta 2007;52: 4287–98.

[30] Jiang L, Sun G, Zhou Z, Zhou W, Xin Q. Preparation and characterization of PtSn/C anode electrocatalysts for direct ethanol fuel cell. Catal Today 2004;93-95:665–70.

[31] Boccaccini AR, Cho J, Roether JA, Thomas BJC, Minay EJ, Shaffer MSP. Electrophoretic deposition of carbon nanotubes. Carbon 2006;44:3149–60.

[32] Sieben JM, Duarte MME, Mayer CE. Supported Pt and Pt-Ru catalysts prepared by potentiostatic electrodeposition for methanol electrooxidation. J Appl Electrochem 2008;38: 483–90.

[33] Roth C, Gotees M, Fuess H. Synthesis and characterization of carbon-supported Pt-Ru-WO_x catalysts by spectroscopic and diffraction methods. J Appl Electrochem 2001;31:793–8.

[34] Shukla AK, Arico AS, El Khatib KM, Kim H, Antonucci PL, Antonucci V. An X-ray photoelectron spectroscopic study on the effect of Ru and Sn additions to platinised carbons. Appl Surf Sci 1999;137:20–9.

[35] Zhu M, Sun G, Xin Q. Effect of alloying degree in PtSn catalyst on the catalytic behavior for ethanol electro-oxidation. Electrochim Acta 2009;54:1511–8.

[36] Gupta SS, Singh S, Datta J. Promoting role of unalloyed Sn in PtSn binary catalysts for ethanol electro-oxidation. Mater Chem Phys 2009;116:223–8.

[37] Gloaguen F, Léger J-M, Lamy C, Marmann A, Stimming U, Vogel R. Platinum electrodeposition on graphite: electrochemical study and STM imaging. Electrochim Acta 1999;44:1805–16.

[38] Zoval JV, Lee J, Gorer S, Penner RM. Electrochemical preparation of platinum nanocrystallites with size selectivity on basal plane oriented graphite surfaces. J Phys Chem B 1998;102:1166–75.

[39] Plyasova LM, Molina IYu, Gavrilov AN, Cherepanova SV, Cherstiouk OV, Rudina NA, et al. Electrodeposited platinum

revisited: tuning nanostructure via the deposition potential. Electrochim Acta 2006;51:4477–88.
[40] Savinova ER, Hahn F, Alonso-Vante N. The assessment of nanocrystalline surface defects on real versus model catalysts probed via vibrational spectroscopy of adsorbed CO. Surf Sci 2009;603:1892–9.
[41] Gavrilov AN, Savinova ER, Simonov PA, Zaikovskii VI, Cherepanova SV, Tsirlina GA, et al. On the influence of the metal loading on the structure of carbon-supported PtRu catalysts and their electrocatalytic activities in CO and methanol electrooxidation. Phys Chem Chem Phys 2007;9: 5476–89.
[42] Bard AJ, Faulkner CR. Electrochemical methods, fundamentals and applications. 2nd ed. New York: Wiley & Sons Inc.; 2001.
[43] Sieben JM, Duarte MME, Mayer CE. Pt-Ru supported electrodes deposited by multiple successive cycles of potentiostatic pulses: evaluation of nafion film effect on methanol oxidation. J Solid State Electrochem 2010;14: 1555–63.
[44] Wolf D, Yamakov V, Phillpot SR, Mukherjee A, Gleiter H. Deformation of nanocrystalline materials by molecular-dynamics simulation: relationship to experiments. Acta Materialia 2005;53:1–40.
[45] Gootzen JFE, Wonders AH, Cox AP, Visscher W, van Veen JAR. On the adsorbates formed during the platinum catalyzed (electro)oxidation of ethanol, 1,2-ethanediol and methyl-α-image-glucopyranoside at high pH. J Mol Catal A: Chem 1997; 127:113–31.
[46] Sun S, Chojak Halseid M, Heinen M, Jusys Z, Behm RJ. Ethanol electrooxidation on a carbon-supported Pt catalyst at elevated temperature and pressure: a high-temperature/high-pressure DEMS study. J Power Sourc 2009;190:2–13.
[47] Fujiwara N, Friedrich KA, Stimming U. Ethanol oxidation on PtRu electrodes studied by differential electrochemical mass spectrometry. J Electroanal Chem 1999;472:120–5.
[48] Camara GA, de Lima RB, Iwasita T. The influence of PtRu atomic composition on the yields of ethanol oxidation: a study by in situ FTIR spectroscopy. J Electroanal Chem 2005;585:128–31.
[49] Ianniello R, Schmidt VM, Rodríguez JL, Pastor E. Electrochemical surface reactions of intermediates formed in the oxidative ethanol adsorption on porous Pt and PtRu. J Electroanal Chem 1999;471:167–79.
[50] de Souza JPI, Queiroz SL, Bergamaski K, Gonzalez ER, Nart FC. Electro-oxidation of ethanol on Pt, Rh, and PtRh electrodes. A study using DEMS and in-situ FTIR techniques. J Phys Chem B 2002;106:9825–30.
[51] Lamy C, Belgsir EM, Léger J-M. Electrocatalytic oxidation of aliphatic alcohols: application to the direct alcohol fuel cell (DAFC). J Appl Electrochem 2001;31:799–809.
[52] Hitmi H, Belgsir EM, Leger J-M, Lamy C, Lezna RO. A kinetic analysis of the electro-oxidation of ethanol at a platinum electrode in acid medium. Electrochim Acta 1994;39:407–15.
[53] Wang H, Jusys Z, Behm RJ. Ethanol electro-oxidation on carbon-supported Pt, PtRu and Pt_3Sn catalysts: a quantitative DEMS study. J Power Sourc 2006;154:351–9.
[54] Wang H, Jusys Z, Behm RJ. Electrochemical oxidation kinetics and mechanism of ethylene glycol on a carbon supported Pt catalyst: a quantitative DEMS study. J Electroanal Chem 2006; 595:23–36.
[55] Wieland B, Lancaster JP, Hoaglund CS, Holota P, Tornquist WJ. electrochemical and infrared spectroscopic quantitative determination of the platinum-catalyzed ethylene glycol oxidation mechanism at CO adsorption potentials. Langmuir 1996;12:2594–601.
[56] Dailey A, Shin J, Korzeniewski C. Ethylene glycol electrochemical oxidation at platinum probed by ion chromatography and infrared spectroscopy. Electrochim Acta 1998;44:1147–52.
[57] Kowal A, Li M, Shao M, Sasaki K, Vukmirovic MB, Zhang J, et al. Ternary Pt/Rh/SnO_2 electrocatalysts for oxidizing ethanol to CO_2. Nat Mater 2009;8:325–30.
[58] Schauermann S, Hoffmann J, Johánek V, Hartmann J, Libuda J, Freund H-J. Catalytic activity and poisoning of specific sites on supported metal nanoparticles. Angew Chem Int Ed 2002;41:2532–5.